

PAPER

## First lithium experiments in HIDRA and evidence of helium retention during quasi-steady-state stellarator plasma operations

To cite this article: Daniel Andruczyk *et al* 2022 *Plasma Phys. Control. Fusion* **64** 085011

View the [article online](#) for updates and enhancements.

### You may also like

- [Effect of pulse polarity on the temporal and spatial emission of an atmospheric pressure helium plasma jet](#)  
Ruixue Wang, Kai Zhang, Yuan Shen *et al.*
- [XTE J1701462 AND ITS IMPLICATIONS FOR THE NATURE OF SUBCLASSES IN LOW-MAGNETIC-FIELD NEUTRON STAR LOW-MASS X-RAY BINARIES](#)  
Jeroen Homan, Michiel van der Klis, Joel K. Fridriksson *et al.*
- [COMMON PATTERNS IN THE EVOLUTION BETWEEN THE LUMINOUS NEUTRON STAR LOW-MASS X-RAY BINARY SUBCLASSES](#)  
Joel K. Fridriksson, Jeroen Homan and Ronald A. Remillard




**IOP | ebooks™**

Bringing together innovative digital publishing with leading authors from the global scientific community.

Start exploring the collection—download the first chapter of every title for free.

# First lithium experiments in HIDRA and evidence of helium retention during quasi-steady-state stellarator plasma operations

Daniel Andruczyk<sup>1,\*</sup> , Andrew Shone<sup>1</sup>, Zachariah Koyn<sup>2</sup> and Jean Paul Allain<sup>3</sup>

<sup>1</sup> Center for Plasma Material Interactions, University of Illinois at Urbana-Champaign, Urbana, IL, United States of America

<sup>2</sup> Energy Driven Technologies, Champaign, IL, United States of America

<sup>3</sup> Ken and Mary Alice Lindquist Department of Nuclear Engineering, Pennsylvania State University, State College, PA, United States of America

E-mail: [andruczy@illinois.edu](mailto:andruczy@illinois.edu)

Received 15 December 2021, revised 5 June 2022

Accepted for publication 16 June 2022

Published 6 July 2022



CrossMark

## Abstract

Recent experiments in Hybrid Illinois Device for Research and Applications (HIDRA) have had operational discharges between  $t_{\text{discharge}} = 60$  and 1000 s using electron cyclotron resonant heating (ECRH) of the plasma. This means that quasi-steady-state plasma discharges reach conditions to study long-pulse plasma material interactions (PMIs). The newly commissioned HIDRA-Material Analysis Test-stand PMI diagnostic is used to place a drop of lithium onto a heated tungsten surface, transfer the sample in-vacuo and expose it in a helium plasma. Helium is of interest as there is an open question to whether lithium will be able to remove helium ash in real fusion devices. The introduction of the W-Li sample in HIDRA resulted in evaporation of lithium into the helium plasma during a 600 s pulse and caused a reduction of over 90% in neutral pressure during the discharge. It was also observed that the plasma density and temperature increased by over 2.5 times. Using spectroscopy and a helium collisional radiative model, the peak temperature and density of the helium plasma can be monitored during the discharge. During lithium evaporation, as significant lithium ionization occurs, there is a 85% drop in the HIDRA vessel neutral pressure, despite a constant flow rate of He gas. This reduction in neutral pressure is supported by spectroscopy data with corresponding reductions in He I line intensities (587 nm, 667 nm, 706 nm, and 728 nm), as well as those of other impurities. At one point in the discharge a lithium plasma is created, as indicated by an increase in  $\text{Li}^+$  emission and a complete reduction in  $\text{He}^+$  emission, but the electron density jumps from  $n_e = 3 \times 10^{18} \text{ m}^{-3}$  to over  $n_e = 8 \times 10^{18} \text{ m}^{-3}$  while the core temperature stays relatively constant between  $T_e = 16 \text{ eV}$  and 20 eV. Once lithium has completely evaporated from the sample and the majority of the ionized lithium has diffused from the plasma to the vessel walls, pressure and spectroscopy data paired with He collisional radiative model calculations shows a re-establishment of a helium plasma in a low recycling regime. In this regime, the density drops down to  $n_e = 2 \times 10^{18} \text{ m}^{-3}$  and the electron temperature increases from  $T_e = 20 \text{ eV}$  to over  $T_e = 50 \text{ eV}$  indicating an increase in helium heating efficiency. This is also indicated by the  $\text{He}^+$  emission re-establishing and having a higher intensity. In this paper we show the results from the first lithium campaign in HIDRA. In the presence of lithium, and in particular when lithium ions are present, the helium disappears from the plasma via an as of yet unknown

\* Author to whom any correspondence should be addressed.

complex relationship that needs to be further studied. The most likely explanation is that the lithium ions are distributed around the vessel and able to trap helium to the surface turning HIDRA into a large gettering surface. These results have potential implications on future plasma facing component design using liquid lithium for impurity and recycling control using limiters and divertors.

Keywords: HIDRA, helium, lithium, fusion, PMI, plasma

(Some figures may appear in colour only in the online journal)

## 1. Background

The most pressing issue to obtaining an operating fusion reactor is developing the materials of the first wall and divertor. The choice of material for these plasma facing components (PFCs) not only influences the operation of the reactor, but also its design. Over the history of fusion there have been several material candidates ranging from carbon (in the form of graphite) to high-Z materials such as tungsten. Currently the solid materials of choice for the International Thermonuclear Experimental Reactor (ITER) are tungsten and beryllium [1], which are being studied in the Joint European Torus (JET). Tungsten is resilient to physical and chemical sputtering and has low tritium retention [2, 3]. Recent results in JET with the ITER-Like-Wall, however, have shown lower confinement than previously obtained when operating with graphitic PFCs [4].

Tungsten has some other significant problems, including embrittlement due to neutron damage [3, 5], which can have an influence on the properties of tungsten, such as thermal conductivity. In the presence of implanted deuterium and helium, tungsten forms bubbles under its surface and develops ‘fuzz’ structures as the bubbles expand which can cause problems [6, 7]. Bubble bursting releases cold gas into the plasma and possible tungsten dust from fuzz formation [8, 9] which can cause a catastrophic failure of the plasma itself. Ions returning to the plasma after an interaction with the wall is known as recycling. The ions are much colder going back into the plasma compared to their pre-interaction temperature which is a main driver of plasma instabilities and performance issues. Solid PFCs have high recycling coefficients and this material property is potentially a detrimental flaw from a plasma material interactions (PMIs) perspective.

As an alternative to tungsten and other solid materials, lithium offers a solution to several of the problems associated with solid PFCs such as fuzz-growth, recycling behavior, and fuel retention. In particular, it can be flowed as a liquid which avoids permanent damage when exposed to instabilities like edge localized modes (ELMs) and disruptions. Lithium has also been seen to improve the performance of devices, which has been observed in several devices such as TFTR, NSTX, EAST, CDX-U and LTX [10–14]. This has been linked most closely to the fact that recycling,  $R$ , is reduced significantly. As little as a 5% reduction in  $R$  can show a marked improvement in plasma performance [13]. The link between low recycling and machine performance is supported further with experiments in DIII-D where a small decrease in the

recycling was achieved not using lithium, but with a divertor cryo-pump, and a significant increase in the edge pedestal temperature was observed [15]. It has been suggested that with a low recycling regime in a fusion reactor, flat electron and ion temperature profiles can be obtained [16, 17]. If this were to be true, reactor design is significantly impacted, since the whole plasma volume, and not just the inner core, is able to achieve fusion temperatures and thus generate fusion power. This would lead to a significant reduction in the size of a machine. The first experimental evidence of electron temperature profile flattening was seen in LTX where the electron temperature not only increased roughly 1.5 times but flattened out all the way to the last closed flux surface [18].

Lithium, being such a reactive element due to its single valence electron, will bond with impurities in a fusion device. However, describing the mechanisms behind impurity formation is complex and has been studied on metal PFCs in LTX. It was observed, using the Material Analysis Particle Probe (MAPP), that lithium first forms complexes with oxygen and these, in fact, are what trap and hold cold hydrogen, while energetic hydrogen is trapped within the lithium layers at the edge [19]. This provides the ability to hold a low recycling surface well after a discharge is performed [20], enabling lower amount of lithium needed per discharge. Most recently, a large multi-institutional collaboration between the U.S. and China has conducted research using lithium in various forms to help understand and control long pulse plasmas in EAST [21]. A combination of lithium powder droppers, pellet injectors and a flowing liquid lithium (FLiLi) limiter were used to suppress and control ELMs and demonstrate recycling control.

When it comes to recycling and lithium’s ability to trap atoms, another pressing question is what effect does lithium have on helium? As an inert atom, and the by-product of fusion the deuterium-tritium (DT) reactions, helium needs to also be pumped by lithium. Helium itself is an issue for cryo-pumps as even at low temperatures it hardly sticks to surfaces. The implications are that any future liquid lithium divertor system will need to be able to handle helium ‘ash’ that is eventually incident on a PFC or the divertor surface. The helium itself can cause issues with solid surfaces, in particular tungsten where tendrils structures called fuzz can be formed. This can cause arcing and dust into the plasma causing a collapse in the plasma. Also, if not sufficiently removed the helium can be a dilutant of the plasma core reducing the plasma performance and output power. Dealing with helium is an open question, with few studies being performed. One of the first studies was by Hassanein *et al* [22] where they carried out a computational

study of the helium diffusion coefficient needed for helium to be trapped. The most significant experimental studies were performed at the University of Illinois on the flowing liquid surface retention experiment (FLiRE) [23]. At the T-11 tokamak, where lithium was used as a conditioning and getter material, it was also observed that not only H<sub>2</sub> and D<sub>2</sub> were absorbed, but also some He [24]. Another interesting aspect of this study is desorption of H/D and He, with He desorbing at temperatures between 50 °C and 100 °C as opposed to 350 °C–400 °C for H/D. Hirooka *et al* has also shown that He will be released from lithium when stirred [25]. This suggests a possible application in future flowing lithium systems where these three species and tritium may be separated out simply by the application of different temperatures.

Recently, new nano-porous tungsten PFCs have been under investigation using the University of Illinois Hybrid Illinois Device for Research and Applications (HIDRA) device [26]. Though these materials are not specifically the subject of this paper, they provided a high-Z substrate which lithium was applied to. The aim was to expose the W-Li surface to the HIDRA steady state plasma edge, in the process evaporate and ionize lithium within the HIDRA plasma column and measure hydrogen and possibly helium retention by lithium atoms in the solid phase. This was done using the newly commissioned HIDRA- Material Analysis Test-stand (MAT) [27]. This paper will discuss the results of a helium plasma exposure and possible implications to PFC and divertor design in future plasma-burning fusion devices. In particular, the paper will focus on shot 3381, which had the best diagnostic data set to describe the observed behavior. However, on a previous lithium evaporation discharge (shot 3274) the same behavior was also observed, but not all the diagnostic settings were optimized for this type of shot due to the unexpected behavior.

## 2. HIDRA and HIDRA-MAT

HIDRA is a toroidal plasma device designed as a classical stellarator. Though originally built as a tokamak, called the Wendelstein Experiment in Grenoble for the Application of Radio-frequency Heating (WEGA), in France in the 1970's [28], it was converted to a classical stellarator in the early 1980's and moved to the University of Stuttgart, and then eventually to the Max-Planck Institute for Plasma Physics in Greifswald in 2000 and renamed Wendelstein Experiment in Greifswald für die Ausbildung (WEGA). In 2014 was taken apart and put back together over an 18 month period at the University of Illinois at Urbana–Champaign where it was renamed [26]. HIDRA is a five period  $l = 2 m = 5$  stellarator with a major radius  $R_0 = 0.72$  m, vessel minor radius of  $r = 0.19$  m and plasma minor radius between  $a = 0.1$  and 0.15 m. There are 40 toroidal coils that can provide an on axis magnetic field up to  $B_0 = 0.5$  T and four helically winding magnetic coils that provide the twist in the plasma. Plasma heating is achieved via ECRH with up to 26 kW possible, though currently 6 kW is more typical. Plasma temperatures  $T_e = 5$ –15 eV and plasma densities  $n_e$ – $10^{18}$  m<sup>-3</sup> range are typical. The heating uses Bernstein wave heating to exceed the density cut-off of the

2.45 GHz sources [29, 30]. Figure 1 shows a recent photo of HIDRA.

One of the features that makes HIDRA stand out among other devices is that it can operate in quasi-steady state time scales, which is up to 1000 s. This allows for a variety of different plasma scenarios to be studied at a time and the evolution of different phenomena can be studied over long-time scales. HIDRA and its various systems are described by Johnson *et al*, in the following [31] and the on-axis magnetic field has been verified using a direct current (DC) hall probe [32]. The central iota profile was determined in Germany and has also been verified in Illinois [33]. The magnetic flux surfaces have been measured using an electron beam and fluorescing rod technique. A long exposure camera allows images of the flux lines to be superimposed to show the shape of the field and compare it to a ray-tracing program [33]. These show that the ray tracing program (FIELDLINES) is able to predict the shape of the magnetic flux surfaces very well.

As mentioned earlier, HIDRA is a long pulse device that is able to operate from what we define as a short pulse,  $t_{\text{discharge}} < 60$  s, to a long pulse discharge,  $60 \text{ s} < t_{\text{discharge}} < 150$  s, and ultimately up to quasi-steady state discharges of  $150 \text{ s} < t_{\text{discharge}} < 1000$  s. There are several diagnostics used to monitor the performance of HIDRA. Figure 2 shows a typical long pulse discharge in HIDRA. Figure 2(a) shows the current going into the coils and figure 2(b) is the on axis magnetic field. Figure 2(c) shows the calculated central iota that is calculated from [33]. Figure 2(d) shows the total amount of power going into the plasma and figure 2(e) shows the neutral pressure inside the vacuum chamber. The working gas for this discharge is helium and the base pressure is  $p_0 = 6.6 \times 10^{-5}$  Pa ( $5 \times 10^{-7}$  torr). The fill pressure is  $p = 2.7 \times 10^{-3}$  Pa ( $2 \times 10^{-5}$  torr). In the future HIDRA will be switching over to hydrogen and deuterium operations. With the base gas being helium, a line ratio technique [34, 35] in conjunction with a collisional radiative model [36] has been employed with spectroscopy to measure plasma temperature and density. Figure 2(f) shows the plasma density, measured with the line ratio of 667.82 nm/728.13 nm, and figure 2(g) shows the temperature, measured with the line ratio of 728.13 nm/706.52 nm. These values seem to agree well with what was measured on WEGA in Greifswald [37], however, it does currently lack spatial resolution and will need to be confirmed with a fast-reciprocating Langmuir probe. Hence, for the purposes of this paper we will use the temperature and density more to look at the trends rather than use as absolute agreed upon values. As a side point, ion temperatures were also measured in WEGA using a coherence imaging system and ion temperatures up to  $T_i = 1.0$ – $2.0$  eV were measured [38], typically about 10% that of the electron temperatures.

The intention of HIDRA has always been to use it as a base for PMI studies. The plasma parameters generated in HIDRA are indicative of what would be seen in the edge plasma of much larger machines. The poor particle confinement time in HIDRA, on the order of 1–5 ms, means that there will be a significant particle flux at the edge, with modeling suggesting a particle flux on the order of  $10^{20}$ – $10^{22}$  m<sup>-2</sup> s<sup>-1</sup>. This makes

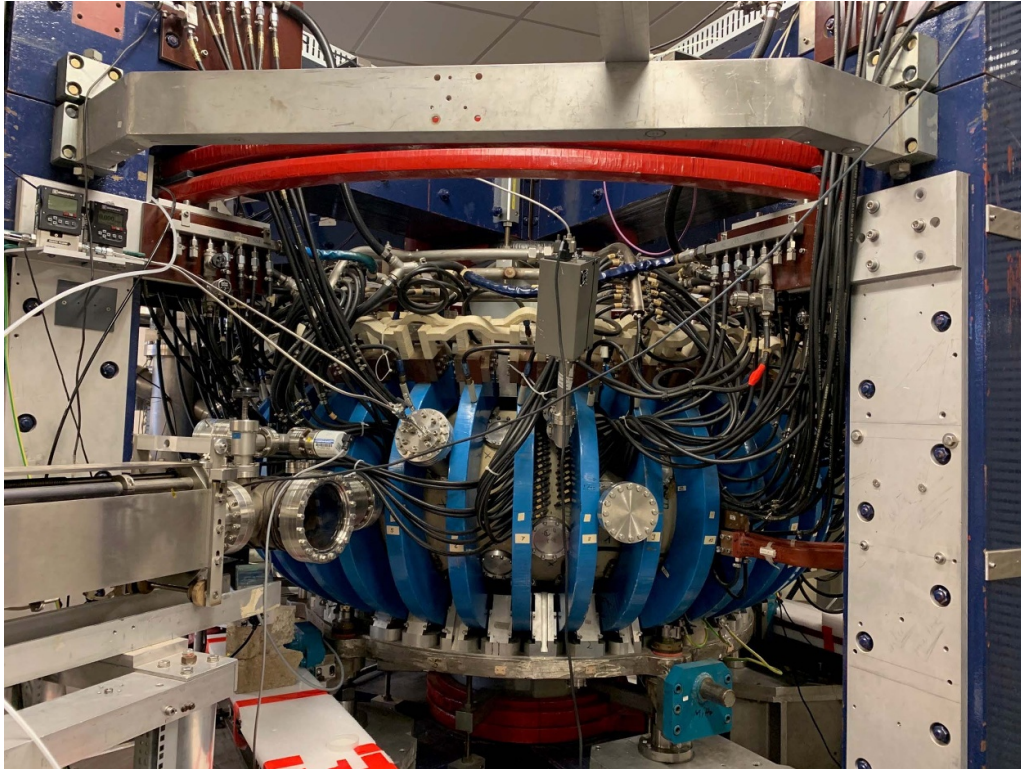


**Figure 1.** Current photo of HIDRA at the University of Illinois. In the foreground is a fast-reciprocating probe and RGA. The aqua blue vertical structures are the toroidal field coils and the large red coils are vertical field coils. The big dark blue structures are the yokes that are part of the Tokamak transformer system [Photo: Courtesy of Daniel Andruczyk].

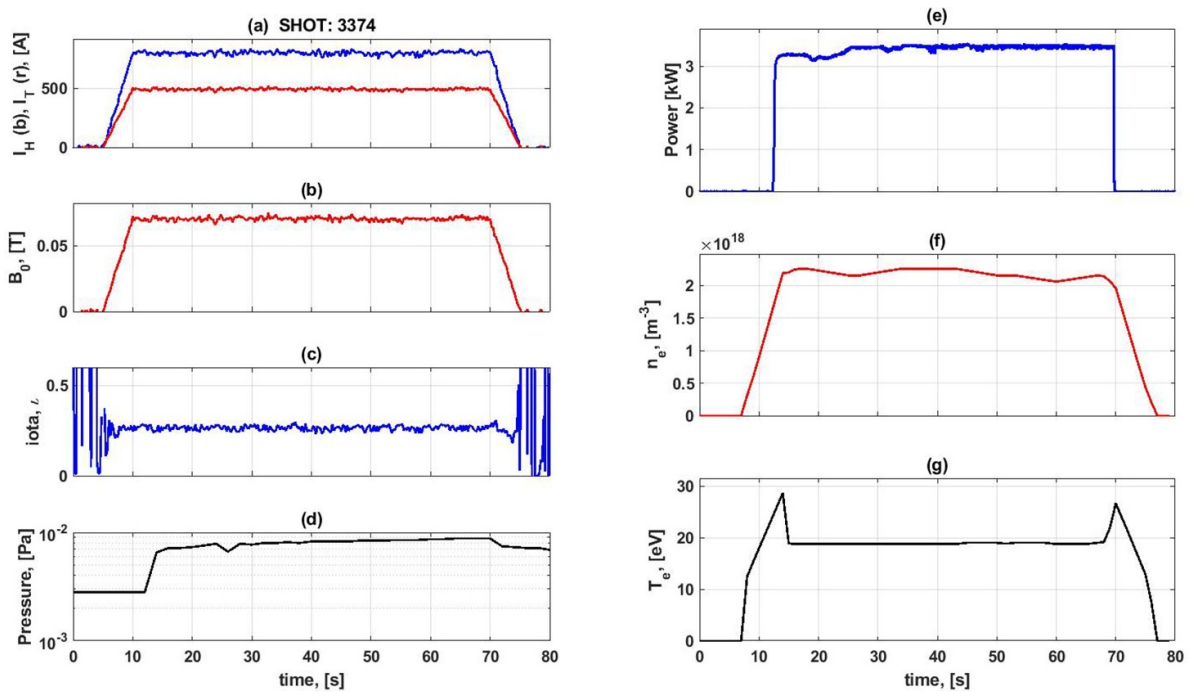


**Figure 2.** Typical HIDRA discharge showing the long pulse operation of the device, where (a) are the currents going into the toroidal (red) and helical (blue) coils, (b) is the on axis toroidal magnetic field, (c) is the calculated on-axis rotational transform from [33], (d) is the neutral gas pressure inside the vacuum vessel, (e) is the net power going into the vessel and thus available to heat the plasma, and (f) and (g) are the plasma parameters plasma density and plasma temperature respectively.

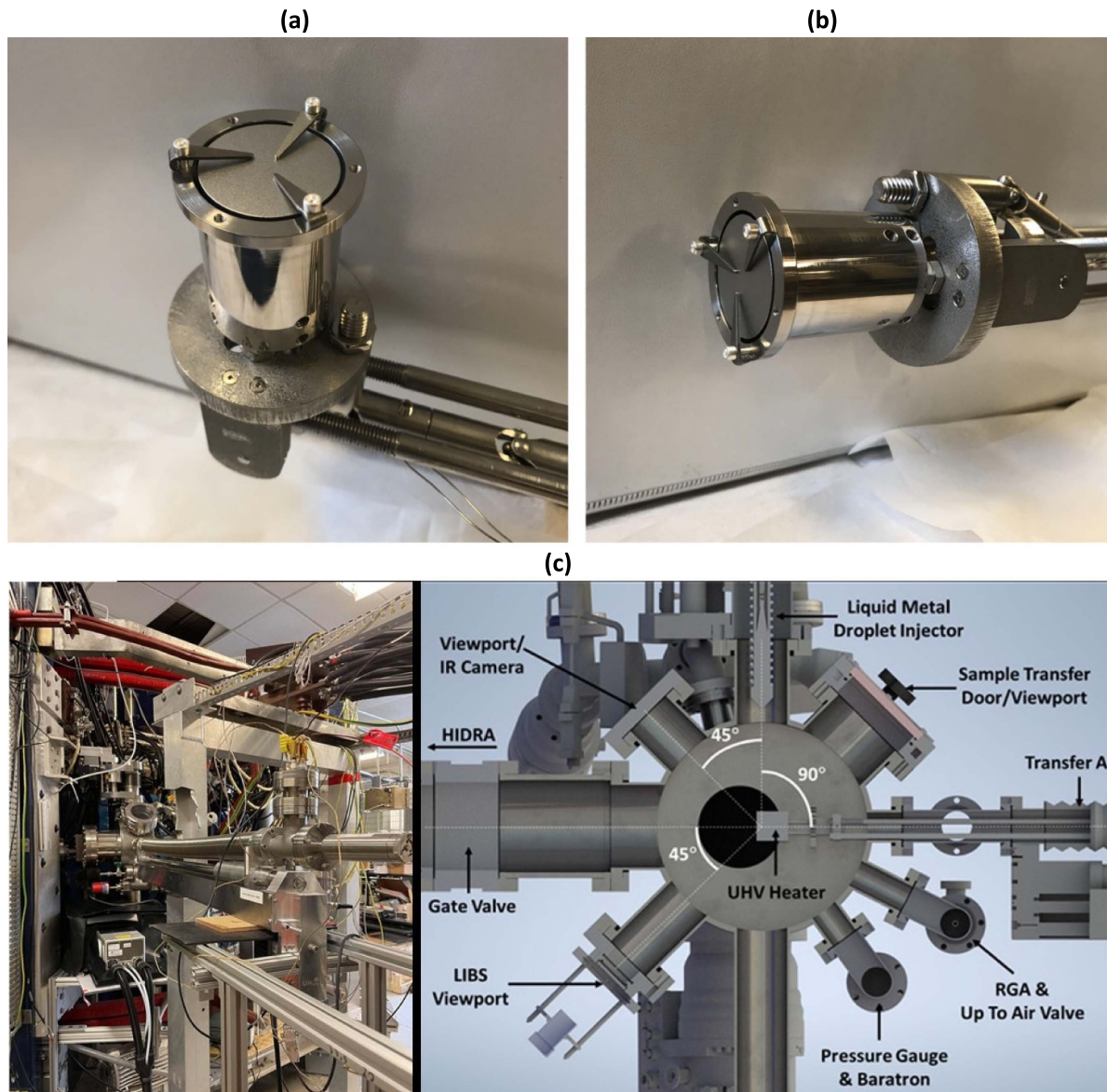


**Figure 3.** The HIDRA-MAT probe heater in its two positions, where (a) is  $90^\circ$  to the direction of travel and allows a lithium droplet to be placed on a surface, (b) is then rotated, ready for insertion into the plasma, and (c) shows a computer aided design (CAD) drawing of HIDRA-MAT and a photo of how it is placed relative to HIDRA.

HIDRA and ideal device to study PMI and to design PFCs and related materials.

### 2.1. Material Analysis Test stand (HIDRA-MAT)

The HIDRA-MAT was developed to utilize the long pulse capabilities of HIDRA and is described by Shone *et al* [27]. The concept is similar to that of the MAPP used on LTX and NSTX [39] in that it provides an *in-vacuo* method to expose samples to the plasma and then do analysis on them without breaking vacuum and thus contaminating any surface effects. Detailed description of HIDRA-MAT can be found in Shone *et al* [27] but one of the main features of HIDRA-MAT is that the sample surface can be rotated  $180^\circ$ , allowing a lithium injector to apply a drop of liquid lithium [40] onto a surface on the probe head *in-vacuo*. The probe head can be heated to ensure wetting

of the surface. The probe head then can be rotated and inserted into the plasma, exposed, and then brought back into the analysis chamber where laser induced blow off spectroscopy (LIBS), laser induced desorption spectroscopy (LIDS) and thermal desorption spectroscopy (TDS) can be performed to analyze the surface for retention of certain species. Figure 3 shows the probe head in its two positions; figure 3(a) is where it would be loaded with a lithium drop and figure 3(b) is when it is rotated ready to go into the plasma. Figure 3(c) shows a computer aided design (CAD) layout of the whole HIDRA-MAT chamber and a current photo of HIDRA-MAT relative to HIDRA. The first experimental campaign for HIDRA-MAT was to observe and characterize the interaction between helium plasmas and lithiated tungsten samples. Specifically, the experiments were to look at helium retention, if any, in the tungsten samples after plasma exposure.

### 3. Experiment

#### 3.1. Experimental setup

HIDRA-MAT was loaded with a 25 mm diameter tungsten disk and held in place with three molybdenum clips on top of an ultra-high vacuum (UHV) button heater. There is a molybdenum heat shield surrounding the UHV button heater along with a stainless-steel shell for mounting and structural support. Before exposure to the HIDRA plasma, the probe head is rotated  $+90^\circ$  to the direction of travel so that the surface could have a drop of lithium ( $\sim 100$  mg) applied to its surface. The sample is then heated to  $290^\circ\text{C}$  to ensure wetting of the sample surface. Lithium application and sample wetting were observed with a camera through a window on the HIDRA-MAT analysis chamber. The sample is then rotated back to its original position. The liquid lithium held onto the surface and did not fall off when rotated.

A LIBS reference shot is performed. This requires the probe head to be rotated  $-45^\circ$  down from the starting position. This LIBS shot is used to provide a baseline for comparison with post-exposure LIBS analysis. Once this is done the sample head is then rotated back to its starting position. It is now inserted into the HIDRA chamber. The probe is inserted 0.145 m into the vacuum chamber and the probe head is placed in an island region of the plasma as is shown in figure 4. This is at a position  $a = 0.045$  m in the vessel and is 0.06 m from the plasma center. The standard configuration of running for this experiment is the  $t = 1/4$  rotational transform. This region of the plasma in some sense can be thought of where the strike point in a divertor would be in a traditional tokamak. Between the islands there is an X-point and thus there will be a high flux of particles bound to some ergodic field lines that will intersect the probe as some point. Part of the probe sample is in the island region where the field lines are more stochastic.

The probe head is exposed to the HIDRA plasma at this point. As mentioned earlier, the plasmas can be anywhere from 10's to 100's of seconds, and even 1000 s. For this experiment, a 620 s discharge was chosen. This includes 10 s before the ECRH is switched on to ramp the magnetic fields up, then a 600 s 'flat top' is maintained, and then 10 s at the end for ramping down the magnetic fields. Once the sample head has been exposed, it is then retracted back into the main HIDRA-MAT chamber where analysis on the surface can be performed.

#### 3.2. Shot 3381

To reiterate, shot 3381 is the second time in HIDRA that a lithium evaporation experiment has been observed to have a significant impact on helium behavior during a plasma. For Shot 3381, which is of interest for this paper, this last step of the procedure (LIBS) was not able to be performed since the PMI was so rigorous on the HIDRA-MAT probe head and sample surface that even the molybdenum clips and

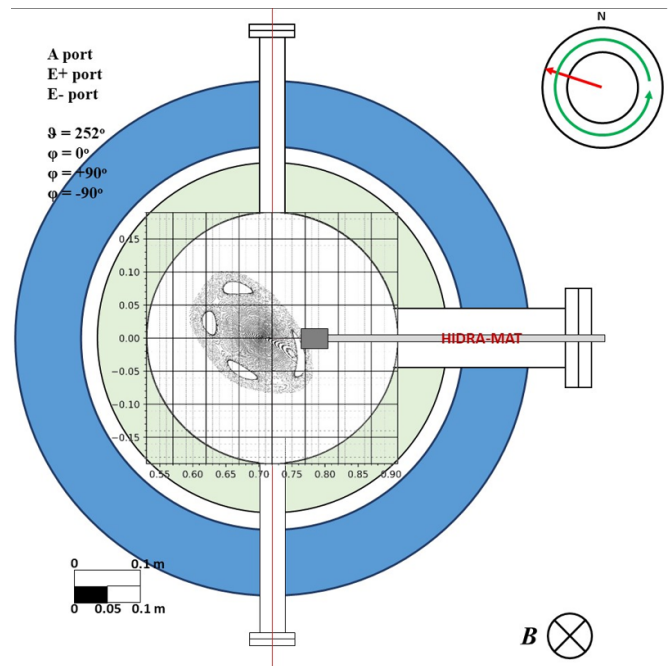


**Figure 4.** Schematic showing the HIDRA-MAT probe head inserted into HIDRA and its position to the plasma edge. In fact, the surface of probe head sits in an island and can be considered to act like an island limiter. The circle in the upper right shows HIDRA-MAT's toroidal position on HIDRA. The thick light green circle is the HIDRA vessel wall and helical coil thickness, and the larger blue circle represents a toroidal magnetic coil.

stainless-steel body were melted and all the lithium was evaporated off the W surface. The 6 kW ECRH antenna was also just within the plasma edge and significant PMI was observed on one corner of the antenna as well. Thus, plasma data is presented, but no surface analysis results are included in this paper.

#### 3.3. Diagnostics

There are several diagnostics used during the experiment to monitor device parameters. Pick-up sensors that are part of the magnetron waveguide measure the forward and reflected power to measure how much actual power is going into the vessel and plasma. A sniffer probe is used to monitor how much of the microwave power is being absorbed into the plasma. This is based on a Hör electronics Messkopf 210 A microwave sensor that is looking directly into the vacuum vessel. This does not give an absolute measurement of the power, but a relative one, where the signal before plasma and during plasma are compared. This gives an indication of the absorption efficiency of the microwaves into the plasma, but not necessarily the efficiency of heating the plasma. Two edge Langmuir probes measure the floating potential during the shot to give an indication of how the particle fluxes are changing outside of the main confined plasma. A color camera also looks into the vessel and is mounted on a vacuum vessel B-port next to

the 6 kW ERCH system. Through this camera the antenna of the 6 kW and 20 kW can be viewed, as well as the plasma. Finally, an Ocean Insight HR2000+ series spectrometer, with a wide range of 200 nm–1100 nm looks at the center of the vacuum vessel. The spectrometer is connected via fiber optic to a 74-VIS collimating lens oriented to collect parallel light from a 5 mm diameter vertical section of the plasma. The spectrometer allows many spectral lines to be observed during the discharge, obtaining time-resolved spectra. A spectrum was recorded every second during the discharge with a 5 ms integration time.

#### 4. Results

Figure 5 shows images of the helium plasma in HIDRA. In particular, it shows images of the plasma from shot 3381. In the first image, this is a typical image seen from a helium plasma with no lithium. Figure 5(b) is taken at about 150 s after the start of the experimental run in shot 3381, which corresponds to 140 s into the discharge flat top. The third image, figure 5(c), is taken at about 250 s into the discharge. All are captured frames from a video of the plasma discharge. A color change of the plasma can be seen with lithium being present, compared to the image in figure 5(a). The bright green color is iconic of the  $\text{Li}^{+1}$  line, 548.6 nm, and the PMI on the antenna is seen as a red glow as well.

The tungsten sample on HIDRA-MAT had a 7.5 mm diameter drop of lithium, which is approximately 113 mg, and was inserted into the HIDRA vacuum chamber before the discharge was switched on. It was placed 0.145 m into the vessel, which puts the sample surface right in the edge of the plasma and in fact touching one of the islands, as shown in figure 4. The sample was then heated to about 290 °C. The tungsten surface itself was textured and non-porous, and thus we see that the surface tension of the lithium is more than enough to hold it in place on the tungsten surface.

Before any experiment, the base pressure inside HIDRA is about  $p_0 = 6.7 \times 10^{-5}$  Pa ( $5.0 \times 10^{-7}$  torr). Then helium with a flow rate of 1 sccm brings the operating pressure in HIDRA up to  $p = 1.1 \times 10^{-2}$  Pa ( $8 \times 10^{-5}$  torr). The surface of the sample was heated to 290 °C to ensure that the surface at some point would exceed the evaporation temperature of 400 °C, as lithium's effects on plasma operation were of particular interest. Previous experiments where the surface was heated below 200 °C at the start of plasma exposure showed little to no lithium evaporation into the plasma.

The discharge procedure is as follows: the first 5 s there is no current in the magnetic coils and is used to serve as a baseline for the experiment. The current is then ramped up in the magnetic coils to their designated values over 5 s, and then the rest of the discharge is referred to as the 'flat top' is where experiments are performed. After 610 s the current to the magnetic coils ramps down over 5 s and then another 5 s is run without current as another baseline. The magnetron heating comes in just after 10 s into the experiment once the magnetic coil currents have reached their designated values.

The magnetic coil currents for this experiment are  $I_T = 468$  A and  $I_H = 790$  A, which correspond to a central rotational transform value of  $\tau = 0.264$ . This is the  $1/4$  rotational transform with four islands in the edge. The pressure of the vacuum vessel is monitored via a Pfeiffer Vacuum Full Range gauge. The spectrometer is looking directly into the center of the vacuum chamber, however, FIELDLINES tracing and electron beam measurements, as well as past measurements in Greifswald, show that the plasma center is about 15 mm towards the high field side and has a hollow profile [33, 37]. Thus, until further measurements of the electron density and temperature profile across the plasma using a Langmuir probe can be taken, the values of electron temperature and density are used in discussion with the understanding that more diagnostic data has to be collected. When compared to the values reported in Horvath *et al*, though, the presented values are reasonable [37].

Figure 6 shows an example of the spectrum seen by the spectrometer. The spectrometer is triggered every second over the length of the discharge with the integration time of 5 ms. This value was determined in previous test discharges where it was seen that the light intensity was very strong. Figure 7 shows data for shot 3381.

There are four helium lines of specific interest that are monitored. The 728.13 nm and 667.82 nm lines are used to calculate the electron density in the collisional radiative model (CRM) and the 706.52 nm and 728.13 nm lines are used to calculate the electron temperature. The 468.53 nm line is the  $\text{He}^{+1}$  ion line. The  $\text{H}_\alpha$  line, 656.28 nm, and neutral oxygen line, 777.42 nm, are monitored since there will be some water vapor in the machine and so these two impurities will be present. Finally, two lithium lines are monitored, the dominant neutral line, 670.78 nm, and the  $\text{Li}^{+1}$  ion line, 548.36 nm. All of these are used to understand how the plasma evolves.

There are five regions of interest that have been identified and tell the story of what is happening in the plasma. It is important to remember that here the hydrogen and oxygen spectroscopic signals are due to water vapor in the chamber. The helium is continuously flowing at 1 sccm into the vacuum chamber. This means that helium is the recycling atom and the hydrogen and oxygen are impurities.

Figure 7(a) shows the current flowing into the toroidal (red) and helical (blue) magnetic coils. Figure 7(b) is the on axis toroidal magnetic field. The central rotational transform,  $\tau$ , for HIDRA is shown in figure 7(c) and is calculated by equation (3) in Rizkallah *et al* [33].

The forward (blue) and reflected power (red) from the magnetron are shown in figure 7(d). The electron density and temperature calculated using the collisional radiative model are shown in figures 7(e) and (f), respectively. The neutral pressure in the main HIDRA vacuum vessel is shown in figure 7(g) and the surface temperature of the HIDRA-MAT probe head is in figure 7(h). There are four black lines shown. The first is 400 °C, which is the temperature where clean lithium will start to evaporate at a pressure of  $1.3 \times 10^{-4}$  Pa ( $1 \times 10^{-6}$  torr). The second line at 650 °C is the lower temperature limit where the  $\beta$  phase of hydrogen bonded to



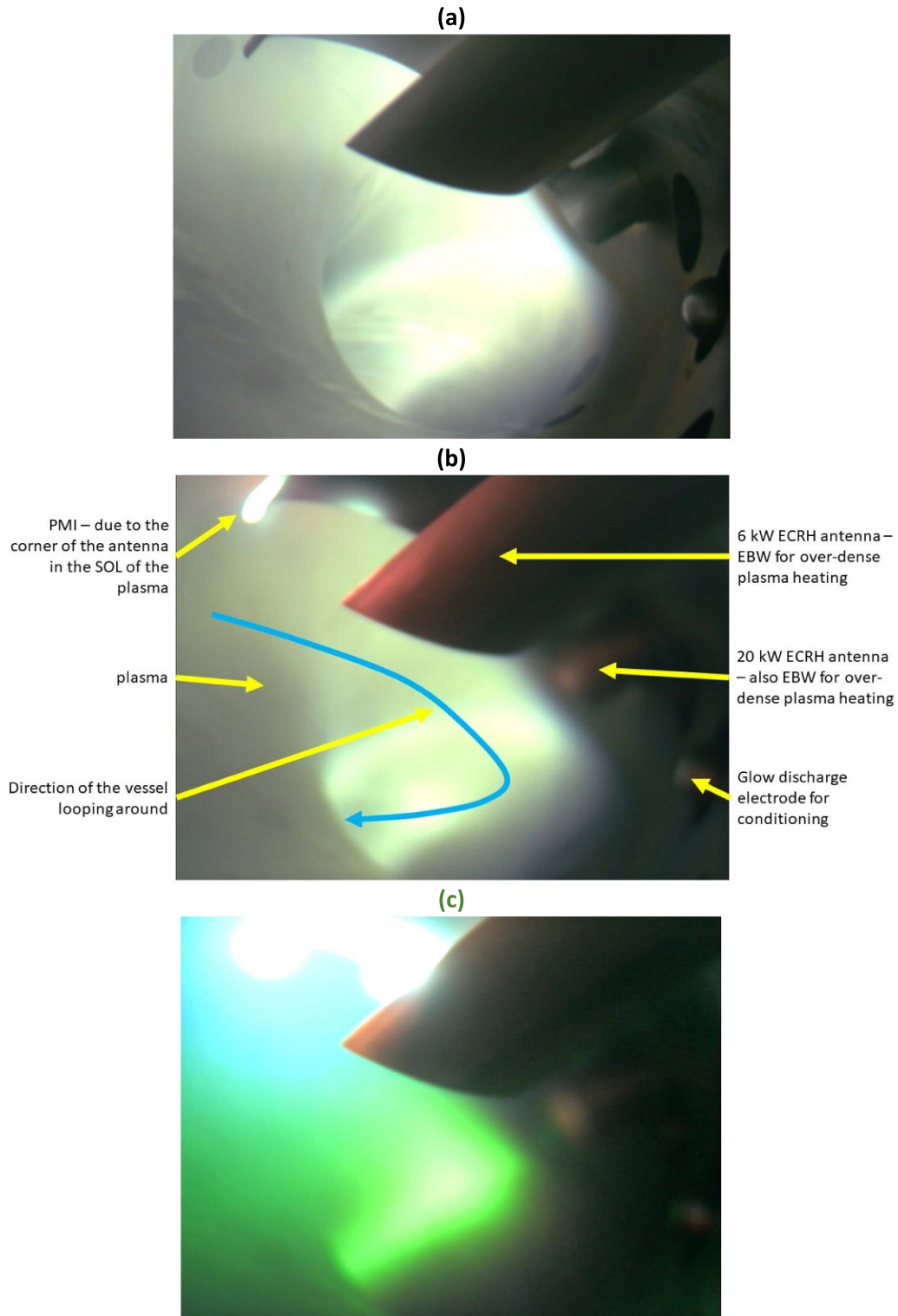


**Figure 5.** Image of the HIDRA plasma, showing (a) a typical helium discharge with no lithium and (b) helium plasma about 150 s into the discharge. The red glow on the antenna is unique to the lithium neutrals and PMI on the antenna is already being observed. Other features in the vessel are also pointed out (c) at about 250 s into the discharge, shot 3381. The green color is unique to the lithium ion emission and the top of the antenna can be seen heating up due to PMI.

lithium (as lithium hydride) will dissociate in lithium and hydrogen and the third line is the upper limit at 690 °C. The final black line is 1200 °C, which is the accurate temperature limit of the thermocouple used to measure the surface

temperature. Figures 7(i)–(k) show the excited helium neutral lines that are used in the CRM but are also a good representation of what the helium neutrals are doing in the vacuum vessel. The helium ion emission line is shown in figure 7(l). The

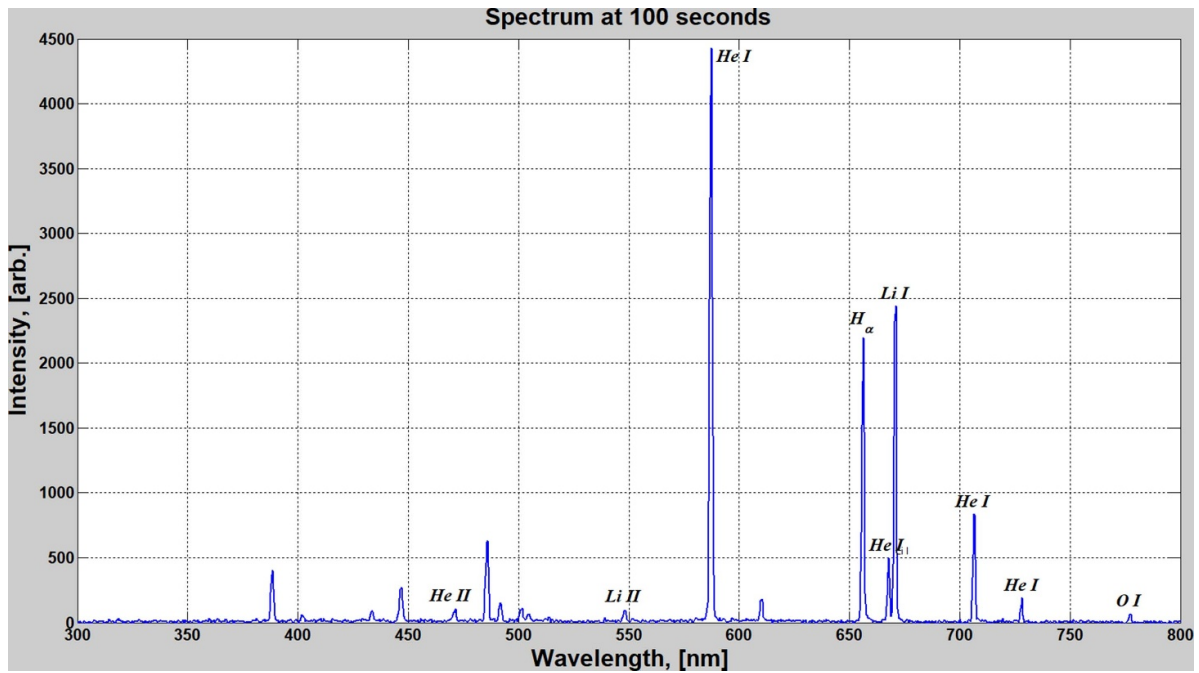


**Figure 6.** Example of the measured spectrum on shot 3381. This was taken at 100 s and some of the spectral lines that are monitored are shown.

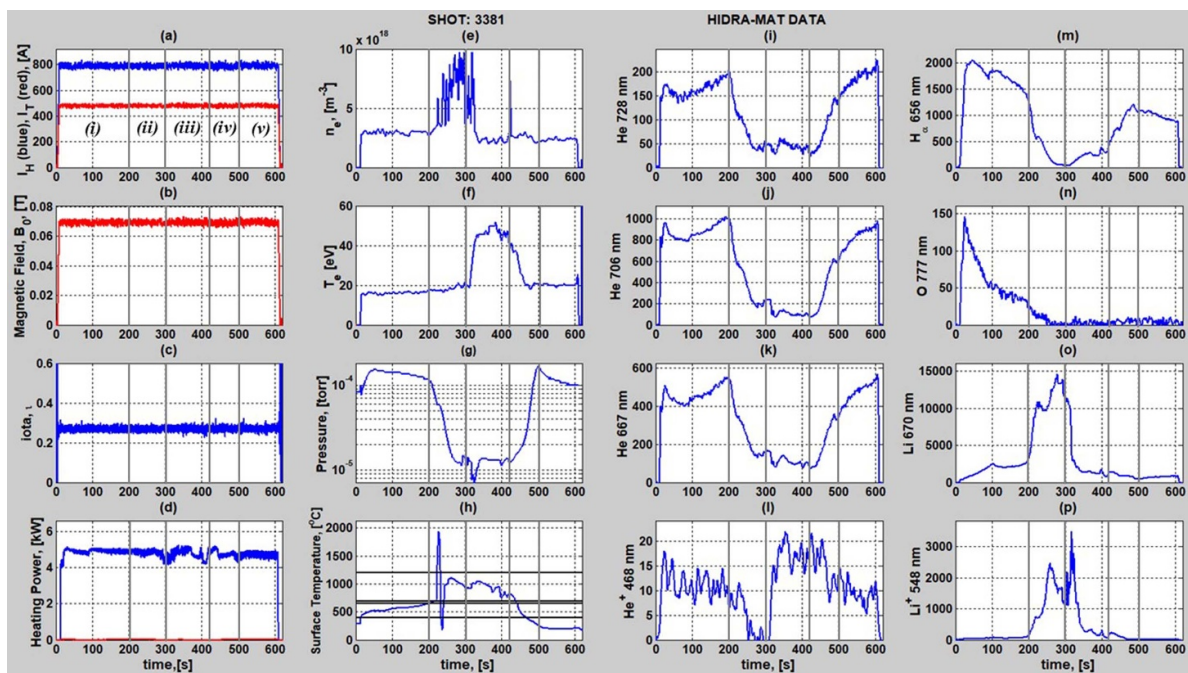


**Figure 7.** Data from shot 3381 showing the 600 s discharge. There are five regions of interest in the discharge that explain what is happening. The first column, from top to bottom shows: (a) the current into the magnetic coils, (b) the on axis magnetic field, (c) central rotational transform value, and (d) the measured microwave power into the vacuum vessel. The second column shows (e) the electron density, (f) electron temperature, (g) neutral pressure in the vessel, and (h) surface temperature on HIDRA-MAT. The third and fourth columns show some of the spectral lines that are monitored; (i-k) are helium neutral lines, (l) is the helium ion line, (m) is the  $H_{\alpha}$  line, (n) is the oxygen line, and (o and p) are the lithium neutral and lithium ion lines, respectively.

hydrogen ( $H_{\alpha}$ ) and oxygen impurity emission lines are shown in figures 7(m) and (n) and the lithium neutral and lithium ion emission lines are shown in figures 7(o) and (p), respectively. The following sections will all be referencing back to these 16 plots in figure 7.

#### 4.1. Region i: 0 s–200 s

The first region of the data corresponds to the opening 200 s. In this region the magnets and magnetron are switched on to generate the plasma. We see that the impurity signals increase as

particles hit the walls and surfaces heat up and eject mainly water, which is then broken down into hydrogen and oxygen. This is seen in the neutral pressure as it jumps from the fill pressure around  $p = 10$  mPa up to almost  $p = 20$  mPa. The probe surface temperature jumps up from 290 °C to 500 °C, and at this temperature and pressure clean lithium will start to evaporate [41]. However, the lithium signal does not have a sharp rise indicating evaporation. It is most probably because the lithium surface is passivated and has a higher vapor temperature.

Further on there is an increase in lithium into the plasma and it is starting to react with impurities which is seen in a decrease of the hydrogen and oxygen lines. There is also small amount of lithium being ionized and we start to see an effect of this on the helium atoms from an increase in the helium lines. The combination of the impurity removal and stub-tuning in this region allow for heating efficiency of the plasma to increase, thus causing the helium line intensity to increase.

At about 100 s the significant decrease in the hydrogen and oxygen signal continues, and in both regions, the neutral pressure is also decreasing. We attribute this to the fact that these impurities are being removed as they are generated. As the neutral background pressure is dominated by the helium neutrals, we do not see much change in the electron density and temperature. Around 180 s into the discharge we do start to see an increase in the lithium signals in both the Li and  $\text{Li}^{+1}$  lines. Up to this point the neutral lithium lines were significant and the lithium ion line was almost nonexistent. The increase in both intensities at 180 s corresponds to the surface of HIDRA-MAT reaching 670 °C [42]. With the increase in lithium, we start to see a drop in the helium signal.

#### 4.2. Region ii: 200 s–300 s

At 200 s there is a significant increase in the lithium neutral emission, which corresponds to a further extreme drop in the  $\text{H}_\alpha$  and O signals. However, the helium neutral emission also decreases significantly, which is seen also in the neutral pressure. It is at this point the lithium ion emission also increases significantly. A reduction in the helium ion line is also seen. Here we also start to see a slight rise in the electron density as well as a very slight increase in electron temperature. At 220 s there is a large spike in the surface temperature on HIDRA-MAT. It is inferred that most of the lithium evaporates off the surface because of the high surface temperature, small amount of lithium, and large increase in Li and  $\text{Li}^{+1}$  lines at that time. At this point it is suspected that the thermocouple that that was on the surface has either shifted or been damaged, as the temperature has far exceeded the 1200 °C it was rated for. Thus, the temperatures read after this time are also only taken as a guide.

At 220 s there is a continued reduction of the helium as the lithium ion emission line rises, while at around 260 s the lithium neutral, though high, goes low, as the ion line peaks. But then these swap as the lithium neutral line peaks in the latter part of the time period and the lithium ion line drops. We see that with the decrease in the lithium ion line, a slight increase in the helium signals occurs. At this point the electron

density spikes to over  $n_e = 8 \times 10^{18} \text{ m}^{-3}$  and we attribute this purely to the fact that there is an increase in the lithium ions and these extra electrons are due to this. Effectively, a lithium plasma is being created at this time from the lithium that has evaporated off the tungsten. The other evidence that this is a lithium plasma is that the helium ions essentially disappear by 300 s. The electron temperature increases to about  $T_e = 22$  eV, since the background neutrals are reduced, and at this point have leveled off at  $p = 0.15$  mPa ( $1.1 \times 10^{-6}$  torr), which is allowing better heating efficiency of the electrons. A reduction in the sample surface temperature is also seen.

Here we also see a significant spike in the surface temperature. Its estimated that temperatures have reached beyond that of molybdenums' melting temperature as the molybdenum clips melted, see figure 9(a)–(c). Also damage and melting of the probe and antenna is observed, seen in figure 9(d).

#### 4.3. Regions iii: 300 s–420 s

The next region begins around 300 s. It is thought that the lithium on the surface of the tungsten sample has been completely evaporated by 330 s. The temperature on the surface of HIDRA-MAT is beyond 690 °C and the significance of this will be discussed in the discussion section. At 300 s the electron temperature starts to rise, and the electron density starts to decrease up to 330 s. Also corresponding to this is that the helium ion emission line starts to return, which means that the lithium plasma is once again being replaced by a helium plasma. Helium is still flowing at 1 sccm the whole time. At 330 s the lithium neutral and ion lines drop but stay at a significant level compared to the start of the whole discharge.

At 330 s the electrons are being heated much more efficiently by the ECRH. At the same time the helium neutrals, that is the recycling atoms, are still very low. This essentially demonstrates a low recycling discharge. The temperature increases from 22 eV to 50 eV and peaks at 55 eV. With the reduction of lithium in the plasma, the remaining lithium ions are likely either confined or lithium that is being sputtered off the walls and re-ionized. A further reduction in the helium neutral signal is seen due to this, however, with the electrons being hotter, the helium ion line increases again. The  $\text{H}_\alpha$  starts to increase since it is tied to the lithium neutrals and with their reduction. This is the case right up to 420 s.

#### 4.4. Regions iv: 420 s–500 s

At 420 s–500 s, the electron temperature drops back to 20 eV, which is slightly higher than at the start of the discharge. At this time, we see that the lithium ions start to reduce, and the helium neutrals start to return, returning to a high recycling plasma. This is seen not only in the pressure but also the emission lines as the emission of the helium ion line flattens out. Towards the end of region four, that is around 450 s, the lithium ion line essentially drops to zero. However, the lithium neutral line is still present. Even though the lithium neutral emission is going down, it does not go away completely and there is an increase in  $\text{H}_\alpha$  accordingly.

The most striking thing is that the disappearance of the lithium ion line corresponds to a rapid increase in the neutral helium signal. Helium is flowing constantly this whole time at 1 sccm. We also see the neutral pressure rapidly rise and initially to the same level as when the plasma was switched on. The electron density, now a truer indication of the plasma density rather than what is contributed from the lithium ions, has dropped to  $n_e = 2 \times 10^{18} \text{ m}^{-3}$ .

#### 4.5. Region v: 500 s–620 s

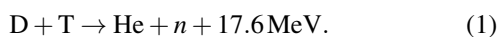
Finally, region V is the last 100 s or so of the discharge. Here we see that the lithium neutrals are still present, and hence we see that the  $H_\alpha$  impurity level is dropping again, which also corresponds to a drop in neutral pressure. This shows the pumping, and low recycling aspects of lithium. At 610 s the ECRH is switched off and the magnetic coil currents are ramped down to finish the discharge. Figure 8 shows some images at different times during the discharge showing how the plasma evolved through the 620 s.

## 5. Discussion

### 5.1. Implications of low recycling operation

The gettering and low recycling abilities of lithium are well known. Using lithium to control oxygen impurities as well as cold hydrogen coming off walls and PFC surfaces before, during, and after a discharge has been observed in several tokamak devices including NSTX [43–45] and EAST [21, 46, 47]. The complex surface chemistry has also been demonstrated in controlled single-effect *in-situ* experiments and modeling [39, 48]. It has been seen that using lithium and reducing the recycling rate directly suppresses ELMs [43, 49], which can be detrimental to reactor operation, causing damage to the first wall and divertor. The other implication is that the plasma temperature will flatten out to the wall as was discussed in the background section. This has been observed in LTX [18] and is also linked to a reduction in the recycling rate. As helium is the main working gas in our experiments, it is thus primarily driving recycling. The hydrogen and oxygen emissions in our case are impurities, but still give much useful information in terms of future hydrogen operations. It is clear that hydrogen and oxygen do react with lithium and are removed, which is seen as a reduction in the neutral pressure in the first 200 s of the discharge. This supports the observations in the [18, 21, 43–47, 49, 50].

What is observed in HIDRA is that helium, being the main recycling element, is also being pumped by the presence of lithium (likely in the solid phase) and appears correlated to an increase in Li ions present in the vapor phase. This exact mechanism is yet to be determined and further study is needed. The implications here are clear, however, since one of the main byproducts of the DT fusion reaction is a helium doubly ionized atom (or alpha).



Once it has deposited its energy into the plasma and recombined to form a neutral helium atom, there is then a potential mechanism observed in these experiments using HIDRA-MAT for the helium to be removed as an impurity from the main plasma and vessel. If the helium can be captured by a flowing lithium surface, then this can be transported out to another external chamber and processed, similar to the FLiRE experiments [23]. Figures 8(a)–(c) show fairly typical helium discharges in HIDRA. However, in figures 8(b) and (c) there is red emission on the antenna surface from lithium neutrals hitting the surface. Also, the PMI of the antenna corner is visible. Figures 8(d) and (e) show 280 s and 293 s, when the lithium ions are present and the lithium plasma is developing, as demonstrated with the green emission of the lithium-ion line. The PMI on the antenna is very rigorous at this point. Figure 8(f) shows the ending of the lithium plasma, which then turns back into a helium plasma. At 380 s is the peak in the electron temperature and helium ion emission, which is where the plasma is the hottest. It is clear to see that the PMI is greater than on the previous images due to the hotter plasma. At this point the camera is starting to become saturated from the intense light coming from the PMI on the antenna and is difficult to see clearly, but in figures 8(g) and (i), the plasma emission has gone back to being like the helium plasma at the start and the PMI is less rigorous.

### 5.2. Where did the helium go?

Lithium neutrals can pump oxygen and hydrogen, which are present due to water vapor in the HIDRA vacuum vessel, in the condensed phase. The implication is that a hydrogen plasma will likely have very low recycling with sufficient lithium present. This is evident as indicated by a decrease of  $H_\alpha$  and O emission lines correlated with the appearance of lithium neutral emission. The reduction in these emission lines the neutral pressure in the first 200 s, and the last 100 s, demonstrates the ability for a lithium plasma-facing interface to pump oxygen and hydrogen in HIDRA. Furthermore, the Li neutral line (Li I) remains present, and the Li ions (Li II) disappear with an accompanying decrease in the  $H_\alpha$  signal. This is indicative of a hydrogen pumping channel related to the presence of lithium at the surface despite the decrease of a lithium plasma. The question still remains about the recycling behavior of helium given this is a helium plasma.

In the beginning 200 s where the hydrogen and oxygen impurities are being removed, it is clear that the helium signal is on the rise, and this is reflected in the electron temperature as well. But between 200 s and 350 s when the lithium ions appear, not only is there a strong reduction in impurities but also in helium. This is seen not only in the neutral pressure in figure 7(g) but also in the helium lines in figures 7(i)–(k). Further evidence that the lithium ions are having an influence on the helium is that at 320 s the lithium neutral signal is decreasing, but there is a large spike in the lithium-ion signal that corresponds to a further decrease in the helium signal and neutral pressure.

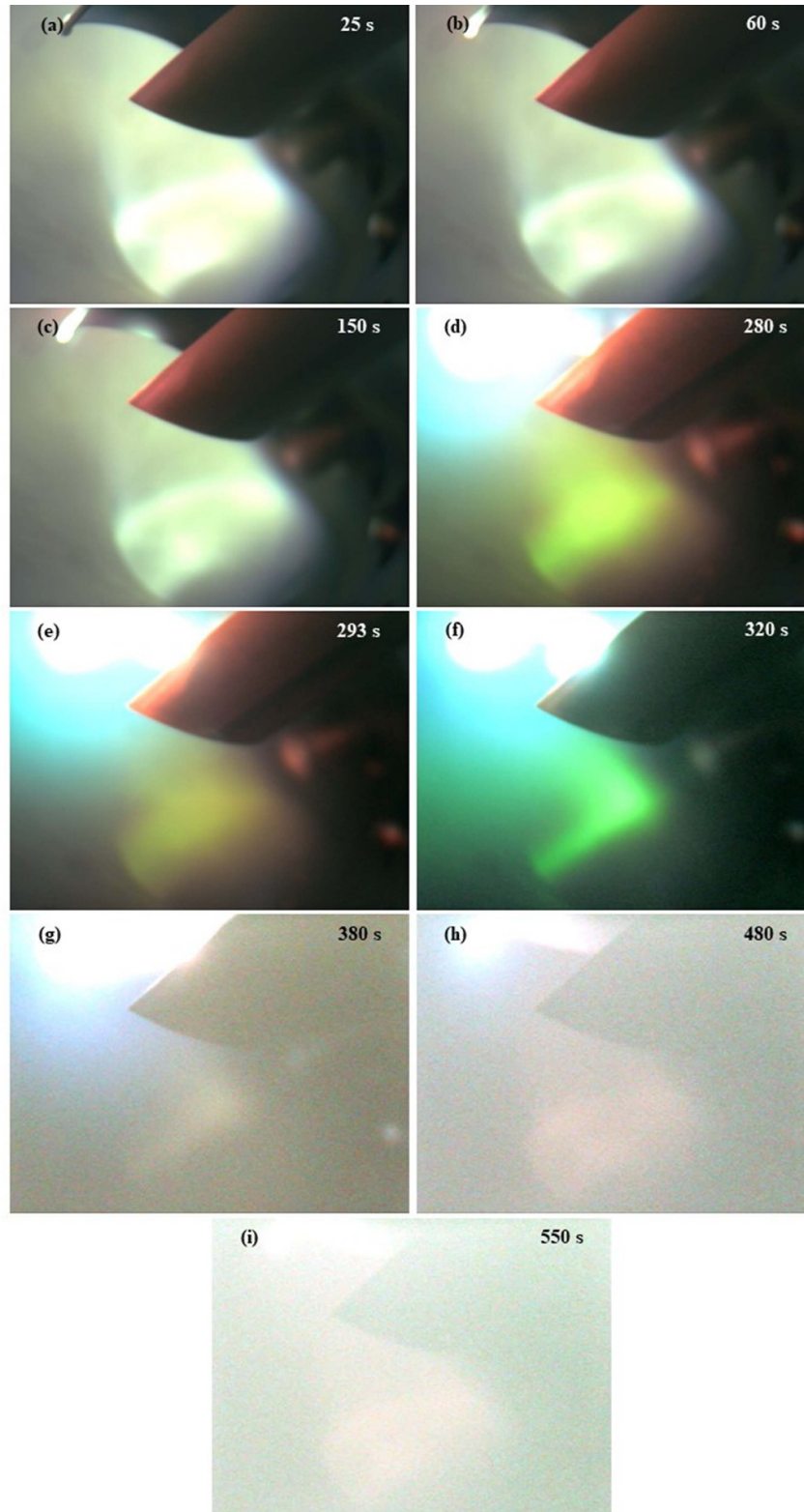


**Figure 8.** Images of the plasma from the camera, where (a) is 25 s at the beginning of the discharge, (b) is at 60 s where lithium is starting to evaporate into the plasma, (c) is 150 s in the middle of section 3 where impurities are being reduced, (d) is at 280 s in section V where the neutral He pressure is at a minimum, (e) is 293 s where the lithium runs out on the W surface at HIDRA-MAT, (f) is 320 s where, despite no more Li on the surface, the Li intensity spikes from Li<sup>+</sup> either confined or coming off the walls and reionizing, and (g)–(i) are at 350 s, 480 s, and 550 s, where the camera is starting to be washed out and hard to make out what the plasma is doing. PMI with the 6 kW antenna is seen.

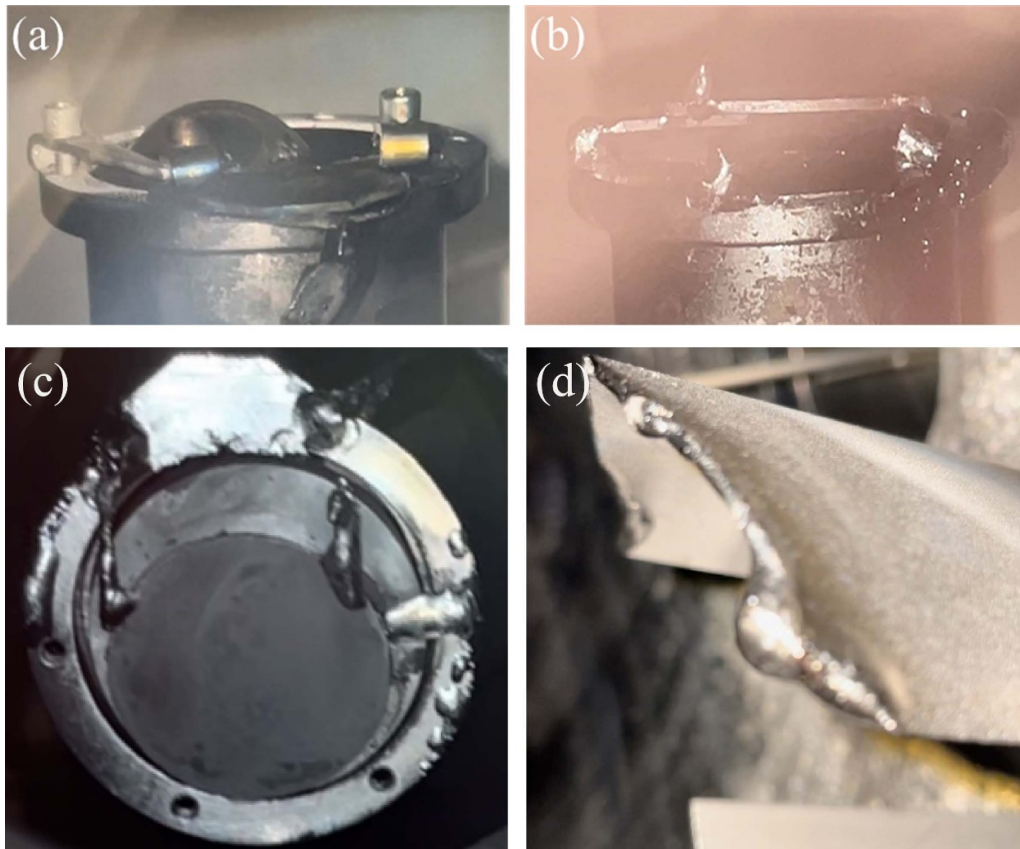


**Figure 9.** Images of the HIDRA-MAT probe surface, sample, and 6 kW antenna after the lithium experiment. (a) In HIDRA-MAT with lithium droplet before insertion into HIDRA. The clips holding the sample are made of molybdenum. (b) and (c) show a side on view of the probe head after the plasma and (d) is the 6 kW antenna edge melted after exposure to the plasma with lithium.

The hydrogen signal does not increase, however, and in fact it is increasing because the amount of lithium neutrals has decreased. At 420 s, the lithium ions start to disappear, and we see the gradual return of the helium and neutral pressure signal. With the return of high recycling the temperature of the plasma drops to 20 eV. The return of the high recycling is also knocking impurities off, and the hydrogen signal increases some more with a slight decrease in the lithium neutrals.

In the 200 s–320 s range the helium ions also disappear, however, the electron density increases dramatically with the appearance of the lithium ions, which indicates that a lithium plasma has been formed. However, after 320 s, where the lithium ions decrease, the helium ion signal reappears, and the temperature increases dramatically with the low recycling condition that now exists. The electron density is now reduced to  $n_e = 2 \times 10^{18} \text{ m}^{-3}$ , which is probably the true indication of the electrons from the helium plasma. The density at the start of the plasma, before 200 s, included electrons generated out of the ionization of hydrogen and oxygen. With the low recycling condition between 320 s and 420 s allowing much more efficient heating of the electrons, this is also seen in an increase in the helium ion emission. The spectrometer, though, does not have sufficient resolution for doppler spectroscopy to determine the helium ion temperature, but the increase in signal is consistent with the heating of the electrons. This shift at 320 s is a result of the lithium at this point

being completely evaporated off the surface of HIDRA-MAT and, with the absence of the lithium source, the only lithium left is what is trapped in the plasma magnetic fields and that being sputtered off the walls.

### 5.3. Comments on the HIDRA-MAT surface temperature

The HIDRA-MAT surface temperature also tells a significant story. Once the lithium drop is placed on the sample surface, it will start to build up surface impurities. We have seen already that there is water vapor in HIDRA. The lithium placed on the surface at the start of the discharge will be exposed to ambient conditions for several minutes before plasma exposure. This allows hydroxide, hydride, and oxide layers to build up. The surface of the sample starts off at 285 °C and, as soon as the plasma begins, it heats up to over 500 °C in the first 40 s. The reason we do not see a large evaporation immediately is because the surface impurities have a much higher dissociation temperature. For lithium hydride this is between 670 °C and 690 °C and oxides are even higher. The lithium seen in the 0 s–200 s spectroscopy signals is coming from sputtering of the lithium from the helium plasma hitting the surface or evaporation of non-passivated lithium.

At 200 s–220 s the 670 °C–690 °C threshold for lithium hydride is reached and at this point hydrogen is driven off, leaving clean lithium behind. The temperature is now well

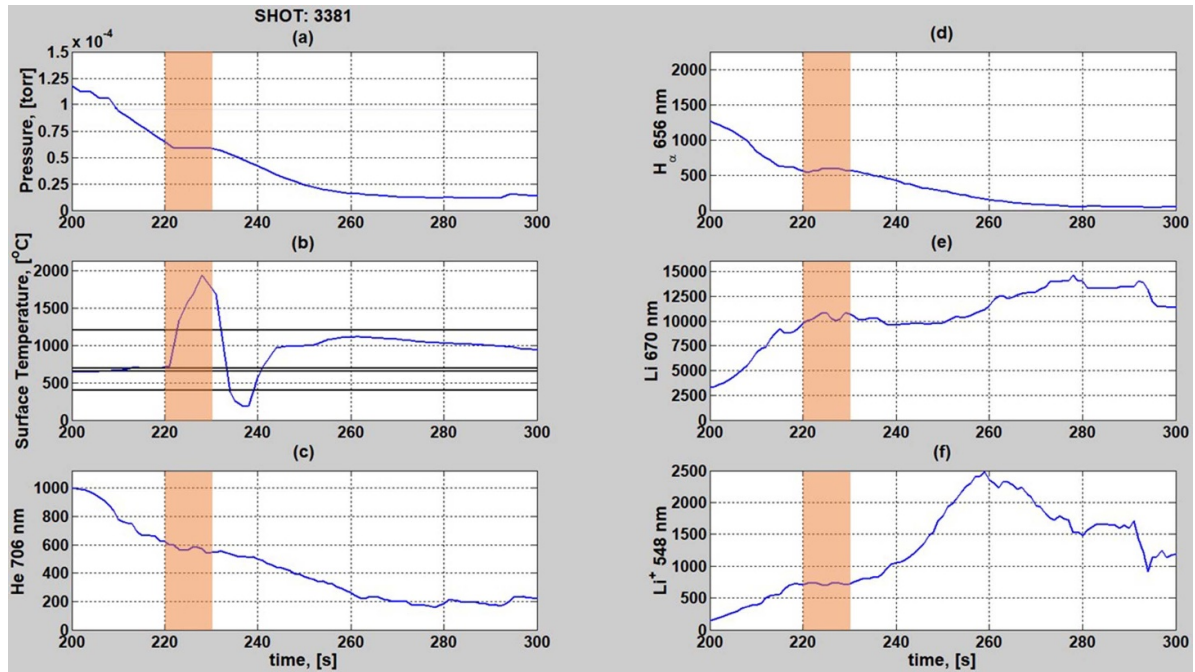


**Figure 10.** Shot 3381 zoomed in between 200 s and 300 s. This shows the plateauing of hydrogen being released from the HIDRA-MAT surface as LiH dissociates at around 670 °C. (a) shown neutral pressure, (b) is the HIDRA-MAT surface temperature with the black lines indicating the same temperature ranges as in figure 7, (c) is one of the neutral helium emission lines, (d) is the  $H_{\alpha}$  lines for the hydrogen impurity, (e) is the Li neutral emission, and (f) is the  $Li^{+}$  emission.

beyond the evaporative limit of lithium and the lithium start to evaporate. We then see spike in the surface temperature to well over the 1200 °C limit of the thermocouple. Furthermore, if one looks closely at the surface temperature from 210 s–220 s, there is a plateauing of the temperature where the hydrogen is being driven off, and in the  $H_{\alpha}$  emission line there is a corresponding plateauing of the signal several seconds later from 220 s–230 s. This is also seen in the neutral pressure curve where there is a corresponding plateauing, shown in figure 10. One possible explanation for this is that the hydrogen that is driven off from the lithium takes several seconds to distribute around the vacuum vessel and reach the pressure gauge on the opposite side of HIDRA. This slight increase is what causes the plateau in the hydrogen signal and pressure curve. However, this effect will need further investigation.

#### 5.4. Possible implications for reactor and PFC design

The mechanism for the helium being removed is still an open question and further experiments will need to be performed to understand the exact mechanism. However, it is most probable that helium in the presence of lithium is being removed at the wall interface. One possible explanation is that with the creation of lithium ions, lithium is more effectively distributed around the HIDRA vacuum vessel because the ions will travel along the magnetic field lines. As the ions travel, they eventually escape confinement, neutralize, and get stuck on the walls due to lithium's high sticking coefficient. This flux of lithium to the walls makes the whole surface of HIDRA one large getter. In the process, the helium atoms are trapped by the lithium on the walls of HIDRA. This would mean that the ratio

of lithium wall coverage to vacuum vessel surface area would be an important factor. A larger machine would require a large volume of lithium to see the same effects. The droplet of lithium, when first placed on the tungsten surface, is essentially spherical and has a diameter of approximately seven millimeters. This means the mass of lithium in the HIDRA vessel is about 113 mg. The surface area of HIDRA is  $S_{\text{HIDRA}} = 5.4 \text{ m}^2$ , which gives a Li mass to device surface area ratio of:

$$R_{\text{ms}} = \frac{113 \text{ mg}}{5.4 \text{ m}^2} = 20.9 \text{ mg m}^{-2}. \quad (2)$$

The amount of lithium needed to put a single uniform monolayer of lithium on the HIDRA surface is about 865  $\mu\text{g}$ , meaning that throughout the exposure there are about 130 monolayers of lithium deposited on the surface of HIDRA. This potentially provides a mechanism for trapping the neutral helium as the lithium is deposited on the surface of HIDRA.

Being able to achieve a low recycling regime for a fusion reactor, one where the plasma temperature is flat (and high) through the whole plasma volume, has massive ramifications for the design of fusion reactors. One can see that a fusion reactor design could have two areas of liquid lithium PFCs. In the first wall a slow flowing PFC could be used to help control the recycling of hydrogen isotopes. The effect of this would be that a device would be able to achieve more fusion product over more of the plasma volume, hence leading to a smaller device [51]. The ramifications are then that the machine would be cheaper in terms of its power and monetary budgets [51]. For example, it has been calculated by Zakharov *et al* that a low recycling burning plasma device could be built at the size scale of JET [52]. This would be a  $P_{\text{DT}} = 23\text{--}26 \text{ MW}$  machine

with a  $Q_{DT}$  of 5–7 [51]. This device is designed to have a slow FLiLi device [53, 54], but could also be just as well built with a LiMIT style device [55, 56] based on thermo-electric magneto hydrodynamic drive [57, 58].

This then leads to the second design of a PFC and that would be a full FLiLi divertor. At the divertor the heat fluxes are the highest and would quickly drive the lithium hot, over 400 °C, and start to evaporate it. Along the scrap-off-layer (SOL) column, one can see that the lithium would be ionized, and it is here at the divertor where the helium would interact with the  $\text{Li}^+$  and be pumped. The helium could be captured and pumped out in the main divertor plenum [59]. The lithium ions would be mainly confined to the region in and around the divertor and should not get back into the main plasma. Thus, it should be feasible to build a full liquid lithium PFC system that can be designed to provide the required particle recycling and helium ash (DT alpha) pumping.

## 6. Future experiments

These results do leave one very open question that needs to be further explored. Though it is clear that lithium, and lithium ions in particular, have a significant effect on helium content in the device, what is the specific mechanism that does this? It is not immediately clear if the lithium ions are pumping the helium or if they provide a transport mechanism for lithium to cover the device walls, which results in either helium trapping due to lithium's large sticking coefficient or lithium layering on the walls. Extra pressure gauges will be added to verify that the same conditions are observed in the neutral pressure. Three residual gas analyzers will be also added and evenly distributed around the HIDRA vacuum vessel to determine whether the helium is really being trapped on the wall or going somewhere else.

HIDRA, with its long pulse, quasi-steady state operation, offers a unique environment to study this phenomenon. In terms of further studies, much more accurate measure of the temperature and density will need to be undertaken. This will require using a Langmuir probe on a fast-reciprocating arm and sampling that plasma at different times during the discharge. The probe will provide radial profiles. It will have a reciprocating mechanism that can insert the probe 9 cm in and out of the plasma in 400 ms. During lithium operation it should be possible to see if the temperature profiles flatten out. As WEGA, the temperature had a hollow profile and densities were peaked [37].

Finally, regarding lithium's ability to pump helium, it would be interesting to see just where the Li–He is being deposited. We postulate that it certainly will be to the walls and propose that HIDRA-MAT be used to diagnose this. A separate lithium heating system will be needed in HIDRA to evaporate the lithium into the plasma to achieve this. HIDRA-MAT will have an unheated sample material, either stainless steel, molybdenum, or tungsten, that will be placed in the plasma edge. Over the course of a discharge the surface will collect the Li–He mixture and, when complete, can be retracted for LIBS, LIDS, and TDS analysis. If the helium is being

pumped to the walls with the lithium, then helium should be observed.

## 7. Conclusions

The first plasma discharges using lithium have been performed in HIDRA. A lithium drop was placed on a tungsten sample on the HIDRA-MAT and exposed to a 600 s helium plasma. Results show that the plasma behavior could be split into two periods. In the first period, lithium is slowly sputtered and evaporated into the plasma. After a long enough time, lithium ions,  $\text{Li}^+$ , are created and the trends in He neutrals change correspondingly. The neutral pressure and helium emission lines decrease significantly with  $\text{Li}^+$  production, as do the oxygen and hydrogen impurity lines. The low background pressure gives rise to a low recycling plasma, allowing for more efficient heating, which increases electron temperature. Since the helium flow rate is constant throughout the whole discharge, we postulate that the  $\text{Li}^+$ –He interaction pumps the helium to the wall.

The second period of the discharge is more complicated: Once the source of the lithium evaporating into the plasma is drastically decreased or non-existent, there is still some lithium in the plasma, either trapped in the magnetic field lines as  $\text{Li}^+$  or ejection or desorption through PMI with surfaces in HIDRA such as the wall and antenna. At 300 s the Li neutral signal decreases, lacking the source of Li neutrals into the plasma, and lithium-ion creation increases briefly because there is more efficient heating of electrons and ionization occurs. This electron-lithium interaction between 300 s and 320 s ionizes some of the Li, leading to a slight increase in electron density and  $\text{Li}^+$  emission. However, once this source of Li is exhausted,  $\text{Li}^+$  concentration drops and the heating power now goes completely into the electrons from the main helium plasma, which has a constant source from the gas flow, hence the large increase in  $T_e$ . As long as there is some  $\text{Li}^+$ , seen between 320 s and 420 s, the electrons are efficiently heated. Once the ions disappear, the background He neutrals start to increase and now the heating is less efficiently coupled into the electrons due to collisions with the higher neutral background. This suggests that the lithium ions distribute around the vessel turning it into a large gettering surface trapping the helium. The consequence is that the electron temperature drops, and the electron density is slightly lower because the overall background pressure is lower due to removal of other impurities by lithium, seen in the  $\text{H}_\alpha$  and O emission lines. The helium signal does not immediately come back to its initial value once  $\text{Li}^+$  content drops, rather it slowly rises from 420 s–600 s. The lithium ions distribute lithium around the vessel turning it into a large gettering surface. If we follow the hypotheses made thus far, with the source of lithium to the walls exhausted, the lithium on the walls would start to passivate and stop trapping the helium. There is also potential that some helium desorbs from the lithium as well.

Thus, the potential implications are that a reactor can be designed to selectively remove helium out of the plasma vessel. This can use a design where there is not just evaporation,



but also ionization of lithium. The incoming helium through the SOL then can be trapped and pumped out with the flowing lithium. The exact mechanism that the lithium ions pumping the helium is still not fully understood and more experiments need to be performed to lock down the exact pathway.

### Data availability statement

The data that support the findings of this study are available upon reasonable request from the authors.

### Acknowledgments

This work is supported by the Department of Energy DOE DE SC0017719, by the University of Illinois Urbana-Champaign Grainger College of Engineering, the Department of Nuclear, Plasma, and Radiological Engineering, the Office of the Vice Chancellor of Research, Facilities, Services at the University of Illinois at Urbana-Champaign. Special Thanks to the ongoing help and discussions from Max Planck Institute for Plasma Physics, Greifswald Germany.

### ORCID iD

Daniel Andruczyk  <https://orcid.org/0000-0001-6613-3509>

### References

- [1] Matthews G F *et al* 2011 *Phys. Scr.* **T145** 014001
- [2] Kessel C E *et al* 2019 *Fusion Sci. Technol.* **75** 886
- [3] Matthews G F *et al* 2009 *Phys. Scr.* **T138** 014001
- [4] Maslov M, Boboc A, Brix M, Flanagan J C, Peluso E, Price C and Romanelli M 2020 *Nucl. Fusion* **60** 036007
- [5] Zohm H *et al* 2013 *Nucl. Fusion* **53** 073019
- [6] Federici G *et al* 2003 *J. Nucl. Mater.* **313–316** 11
- [7] Baldwin M J and Doerner R P 2008 *Nucl. Fusion* **48** 035001
- [8] Ueda Y *et al* 2011 *J. Nucl. Mater.* **415** S92
- [9] Tokitani M, Kajita S, Masuzaki S, Hirahata Y, Ohno N and Tanabe T 2011 *Nucl. Fusion* **51** 102001
- [10] Mansfield D *et al* 1996 *Phys. Plasmas* **3** 1892
- [11] Kugel H W *et al* 2008 *Phys. Plasmas* **15** 056118
- [12] Zuo G, Hu J, Li J, Luo N, Hu L, Fu J, Chen K, Ti A and Zhang L 2010 *Plasma Sci. Technol.* **12** 646
- [13] Majeski R, Doerner R, Gray T, Kaita R, Maingi R, Mansfield D, Spaleta J, Soukhanovskii V, Timberlake J and Zakharov L 2006 *Phys. Rev. Lett.* **97** 075002
- [14] Maan A *et al* 2020 *IEEE Trans. Plasma Sci.* **48** 1463
- [15] West W P *et al* 2002 *Phys. Plasmas* **9** 1970
- [16] Krasheninnikov S I *et al* 2003 *Phys. Plasmas* **10** 1678
- [17] Zakharov L E, Gorelenkov N N, White R B, Krasheninnikov S I and Pereverzev G V 2004 *Fusion Eng. Des.* **72** 149
- [18] Boyle D P, Majeski R, Schmitt J, Hansen C, Kaita R, Kubota S, Lucia M and Roglien T 2017 *Phys. Rev. Lett.* **119** 015001
- [19] Kristic P S, Allain J P, Taylor C N, Dadrás J, Maeda S, Morokuma K, Jakowski J, Allouche A and Skinner C H 2013 *Phys. Rev. Lett.* **110** 105001
- [20] Kaita R *et al* 2017 *Fusion Eng. Des.* **117** 135
- [21] Andruczyk D *et al* 2020 *Phys. Scr.* **T171** 014067
- [22] Hassanein A *et al* 2002 *J. Nucl. Mater.* **307–311** 1517
- [23] Nieto M, Ruzic D N, Allain J P, Coventry M D and Vargas-Lopez E 2003 *J. Nucl. Mater.* **313–316** 646
- [24] Mirnov S V, Lazarev V B, Sotnikov S M, Evtikhin V A, Lyublinski I E and Vertkov A V 2003 *Fusion Eng. Des.* **65** 455
- [25] Hirooka Y, Zhou H and Ono M 2014 *Fusion Eng. Des.* **89** 2833
- [26] Andruczyk D, Ruzic D N, Curreli D and Allain J P 2015 *Fusion Sci. Technol.* **68** 497
- [27] Shone A *et al* 2020 *J. Fusion Energy* **39** 448
- [28] Preinhaelter J and Kopecký V 1973 *J. Plasma Phys.* **10** 1
- [29] Laqua H *et al* 1999 *Plasma Phys. Control Fusion* **41** A273
- [30] Podoba Y Y, Laqua H P, Warr G B, Schubert M, Otte M, Marsen S, Wagner F and Holzhauser E 2007 *Phys. Rev. Lett.* **98** 255003
- [31] Johnson D, Wegley K, Rizkallah R, Shone A and Andruczyk D 2018 *Fusion Eng. Des.* **128** 215
- [32] Rizkallah R *et al* 2018 *IEEE Trans. Plasma Sci.* **46** 2685
- [33] Rizkallah R, Marcinko S, Curreli D, Parsons M S, Bartlett N, Gluck R, Shone A and Andruczyk D 2019 *Phys. Plasmas* **26** 092503
- [34] Schweer B, Mank G, Pospieszczyk A, Brosda B and Pohlmeier B 1992 *J. Nucl. Mater.* **196–198** 174
- [35] Collis S M, Dall R, Howard J, Andruczyk D and James B W 2009 *J. Quant. Spectrosc. Radiat. Transfer* **110** 340
- [36] Goto M *et al* 1997 *NIFS-DATA* **43** 1–80
- [37] Horvath K, Lingertat J, Otte M and Wagner F 2006 *Plasma Phys. Control Fusion* **48** 315
- [38] Chung J, König R, Howard J, Otte M and Klinger T 2005 *Plasma Phys. Control Fusion* **47** 919
- [39] Taylor C N, Heim B, Gonderman S, Allain J P, Yang Z, Kaita R, Roquemore A L, Skinner C H and Ellis R A 2012 *Rev. Sci. Instrum.* **83** 10D703
- [40] Shone A *et al* 2022 *Fusion Eng. Des.* **180** 113193
- [41] Honig R E 1957 *RCA Journal* **2** 195 (available at: [www.powerstream.com/vapor-pressure.htm](http://www.powerstream.com/vapor-pressure.htm))
- [42] Christenson M, Moynihan C and Ruzic D N 2018 *Fusion Eng. Des.* **135** 81
- [43] Ono M *et al* 2000 *Nucl. Fusion* **40** 557
- [44] Maingi R *et al* 2012 *Nucl. Fusion* **52** 083001
- [45] Kaye S M *et al* 2015 *Nucl. Fusion* **55** 104002
- [46] Canik J M *et al* 2018 *IEEE Trans. Plasma Sci.* **46** 1081
- [47] Sun Z *et al* 2019 *J. Nucl. Mater. Energy* **19** 124
- [48] Kristic P S, Allain J P, Dominguez-Gutierrez F J and Bedoya F 2018 *Matter Radiat. Extremes* **3** 165
- [49] Maingi R *et al* 2009 *Phys. Rev. Lett.* **103** 075001
- [50] Alpert D 1953 *J. Appl. Phys.* **24** 860
- [51] de Castro A, Moynihan C, Stemmley S, Szott M and Ruzic D N 2021 *Phys. Plasmas* **28** 050901
- [52] Zakharov L 2019 *Nucl. Fusion* **59** 096008
- [53] Ren J, Zuo G Z, Hu J S, Sun Z, Yang Q X, Li J G, Zakharov L E, Xie H and Chen Z X 2015 *Rev. Sci. Instrum.* **86** 023504
- [54] Zuo G Z, Ren J, Hu J S, Sun Z, Yang Q X, Li J G, Zakharov L E and Ruzic D N 2014 *Fusion Eng. Des.* **89** 2845
- [55] Hu J S, Ren J, Sun Z, Zuo G Z, Yang Q X, Li J G, Mansfield D K, Zakharov L E and Ruzic D N 2014 *Fusion Eng. Des.* **89** 2875
- [56] Ruzic D N, Xu W, Andruczyk D and Jaworski M A 2011 *Nucl. Fusion* **51** 102002
- [57] Xu W *et al* 2015 *J. Nucl. Mater.* **463** 1181
- [58] Shercliff J A 1979 *J. Fluid Mech.* **91** 231
- [59] Maingi R, Watkins J G, Mahdavi M A and Owen L W 1999 *Nucl. Fusion* **39** 1187